

Research Article

TiO₂ and TiO₂-Doped Films Able to Kill Bacteria by Contact: New Evidence for the Dynamics of Bacterial Inactivation in the Dark and under Light Irradiation

John Kiwi,¹ Sami Rtimi,¹ Rosendo Sanjines,² and Cesar Pulgarin¹

¹ Ecole Polytechnique Fédérale de Lausanne, EPFL-SB-ISIC-GPAO, Station 6, 1015 Lausanne, Switzerland

² Ecole Polytechnique Fédérale de Lausanne, EPFL-SB-IPMC-LNNME, Bat PH, Station 3, 1015 Lausanne, Switzerland

Correspondence should be addressed to John Kiwi; john.kiwi@epfl.ch

Received 17 January 2014; Accepted 18 March 2014; Published 5 May 2014

Academic Editor: Cathy McCullagh

Copyright © 2014 John Kiwi et al. This is an open access article distributed under the Creative Commons Attribution License, which permits unrestricted use, distribution, and reproduction in any medium, provided the original work is properly cited.

This paper addresses recent developments in the design, evaluation, and characterization of flexible, uniform polyethylene-TiO₂ (PE-TiO₂), TiO₂-In₂O₃, and TiO₂-polyester able to inactivate bacteria under band gap irradiation and in the dark. The preparation of these bactericide films by sol-gel or by sputtering techniques is reported. The *E. coli* loss of viability kinetics under low intensity and actinic light is evaluated. Evidence for kinetics of the major steps leading to bacterial disinfection in the dark is presented by electron microscopy (TEM). The film surface properties were characterized by surface techniques like EM, DRS, XPS, ATR-IR, CA, AFM, XRD, and XRF. The surface characterization allows the correlation of the film surface morphology with the self-disinfection performance. The events taking place at the cell wall leading to bacterial inactivation when in contact with the TiO₂ films are presented and the steps related to the bond stretching preceding bond scission identified by ATR-IR.

1. Introduction

The ambient contamination by biofilms spreading bacteria for long times in hospitals, schools, and many public places requires the preparation of more effective adhesive antibacterial and *antifungal* films showing an improved kinetics/performance/stability. Antimicrobial nanoparticulate films preparation is a topic of increasing attention since they can reduce/eliminate the formation of infectious bacterial biofilms leading to hospital acquired infections (HAI) [1, 2]. These nosocomial infections are due to antibiotic resistant bacteria. They are becoming more frequent during the last decade and contribute to the increase in hospital care costs. Touching by hand a second person or touching surfaces and walls of hospital deposits bacteria that to a great extent disappear in about 5–8 hours since they do not find the surface humidity or residual C-compounds necessary to feed their metabolism. But there are many and resistant pathogenic bacteria that form stable and robust biofilms secreting proteins to cover/protect themselves and spread

pathogenic bacteria like the Gram-positive *Staphylococcus*. Biofilms are formed from a complex mixture of proteins, saccharides, amino acids, and other extracellular polymeric substances.

The formation of these pathogenic biofilms may be avoided precluded by robust self-disinfecting films. Disinfecting surfaces have been shown to inhibit microbial growth, since bacterial concentrations found in hospital rooms are not high. Regrowth of bacteria was not observed on effective antibacterial films [1–3]. Therefore, the investigation of self-disinfecting surfaces as presented in this study is warranted [4–11].

The colloidal deposition of TiO₂ on textiles, polymers, glass, and steel plates is used to prepare self-disinfectant and self-cleaning surfaces showing a significant photocatalytic activity [12–14]. But the colloid or sol-gel preparations deposited films are not mechanically stable, nor reproducible, and present low uniformity and little adhesion since they can be wiped off by a cloth or thumb [15]. This shortcoming of the colloidal depositions moved us to work on the sputtering

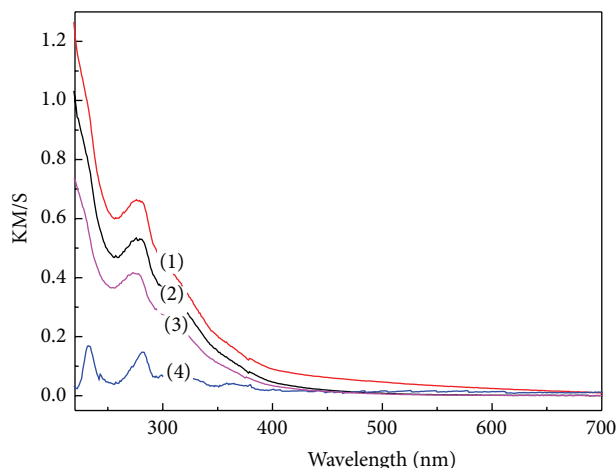


FIGURE 1: DRS in Kubelka-Munk units versus wavelength of TiO_2 sputtered (8 min) on polyethylene: (1) pretreated with UVC 1 torr, (2) pretreated with RF air plasma, (3) pretreated with RF plasma, and (4) TiO_2 sputtered on PE for 1 min.

of antibacterial films to overcome the shortcomings of colloidal loaded films. The problem to fix colloids on surfaces encountered during CVD depositions is due to the heat needed for the film fixation on the substrate. The substrate has to be resistant to heat at temperatures that textiles, polymer films, polyethylene 3D, and polyurethane complex shaped objects do not withstand. Deposition by sputtering of metal/oxides/semiconductors on nonheat resistant substrates is possible since plastic/polymer thin films and textile fabrics can be heated for short times only up to 120–140°C.

In a typical CVD process, the substrate is exposed to the volatile precursors. Due to the heat applied the precursor decomposes on the substrate surface depositing amorphous/polycrystalline coatings. The volatile species condense on the substrate having a lower temperature. The disadvantages of conventional CVD deposition are the high investment costs and the high temperatures needed besides the large amount of heat used requiring costly cooling systems. Recently, Foster et al. [16], Yates et al. [17], Dunlop et al. [18], and Brook et al. [19] have reported antibacterial TiO_2 , Ag, and Cu coatings on glass and polymer films depositing the metal/oxides by CVD.

TiO_2 -films preparation and evaluation have gained much attention during the last decade since they have been reported to be effective in reducing hospital-acquired infections (HAI) [1–3, 20–23]. The particular interest in TiO_2 -textiles is based on the fact that the porous hydrophilic structure as found in cotton textiles provides a suitable environment for bacterial growth. TiO_2 -nanoparticles have shown recently to produce strong antibacterial effects in textiles designed for medical applications [3–18].

The improvement in the performance and utility of antibacterial TiO_2 and TiO_2 -doped films is to produce a film microstructure inducing an accelerated bacterial inactivation concomitant with a cytotoxicity within the accepted standards accepted in medical applications [24–26]. The film uniformity, stable structure, and adhesive properties

are currently investigated by academic institutions and by pharmaceutical companies for medical devices and implants covered with antibacterial coatings [27]. The improvement on the microstructure of TiO_2 films leading to thinner films inducing a faster bacterial inactivation kinetics (doped or not) compared with more traditional DC sputtering and DCP sputtering is being explored in our laboratory. The recent development of highly ionized pulsed plasma magnetron sputtering (HIPIMS) producing high-density plasma to deposit TiO_2 films on polyester is presented in this study [28]. The development of HIPIMS in the last decade is due to the growing demand for high quality anticorrosive uniform films [29]. In the case of HIPIMS, pulses from one microsecond up to milliseconds generate current densities able to induce $\sim 10^{18} \text{ e}^-/\text{m}^3$. This is 10^2 – 10^4 times higher than the electron density obtained by conventional DC-sputtering [30]. Until now, the deposition by direct current magnetron sputtering (DC) pulse sputtering (DCP) and HIPIMS of nanoparticles on surfaces has not been widely used to coat hospital textile clothing, glass, and metal-plates antibacterial surfaces.

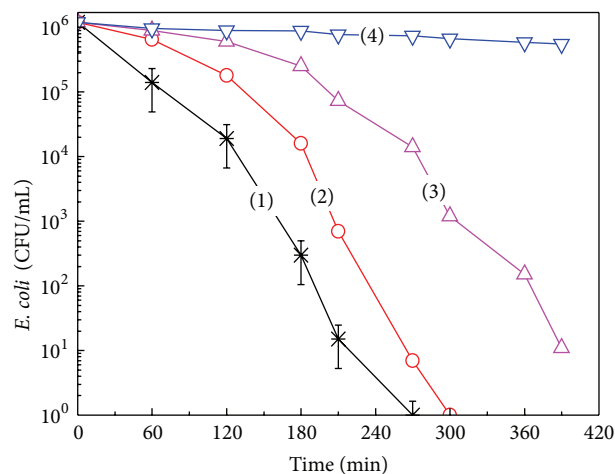
This study will describe results obtained in our laboratory addressing TiO_2 self-disinfection due to (a) transparent non-scattering polyethylene (PE) sputtered TiO_2 films, (b) TiO_2 - In_2O_3 polyester, and (c) nanoparticulate TiO_2 polyester.

2. Materials and Methods

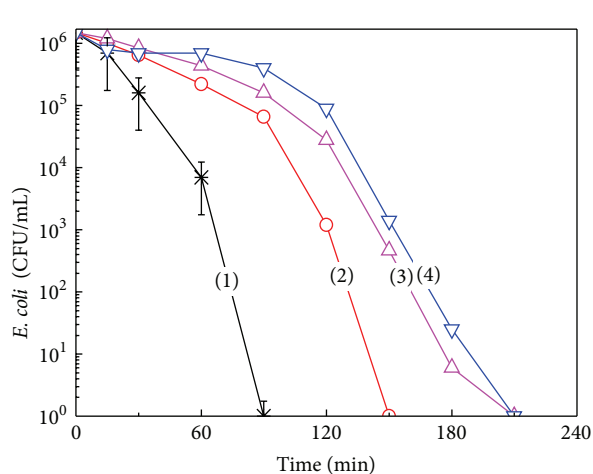
2.1. Sputtering Details, Support Materials, and XRF Determination of Film Loading. The HIPIMS sputtering unit [29, 30] with a CMS-18 Vacuum system from Kurt Lesker Ltd was evacuated to 5.8×10^{-3} mbar. The Ti target was 50 mm in diameter, 99.99% pure from K. Lesker Ltd. UK, and used in reactive O_2 atmosphere. The HIPIMS installation was operated at 500 Hz with pulses of 100 microseconds separated by 1.9 ms, leading to a TiO_2 layer of 15 nm after 60 s. The average power was 87.5 W (5 A \times 350 V) and the power per pulse of 100 microseconds was 1750 W. The calibration of the Ti-film thickness sputtered by HIPIMS was carried out on Si-wafers by a profilometer (Alphastep500, TENCOR). The X-ray fluorescence (XRF) determination of the Ti content in the samples was performed in a PANalytical PW2400 spectrometer.

The low density polyethylene (LDPE) consists of highly branched low crystalline semitransparent film with the formula $\text{H}(\text{CH}_2-\text{CH}_2)_n\text{H}$. The (LDPE) 0.1 mm thick was obtained from Longfellow (ET3112019), had a density of 0.92 g/cm^3 , an upper working temperature of 90°C, and a flowing point of 185°C. The polyester used corresponds to the EMPA test cloth sample number 407. It is a polyester Dacron polyethylene terephthalate, type 54 spun, thickness 130 microns plain weave ISO 105-F04 used for color fastness determinations.

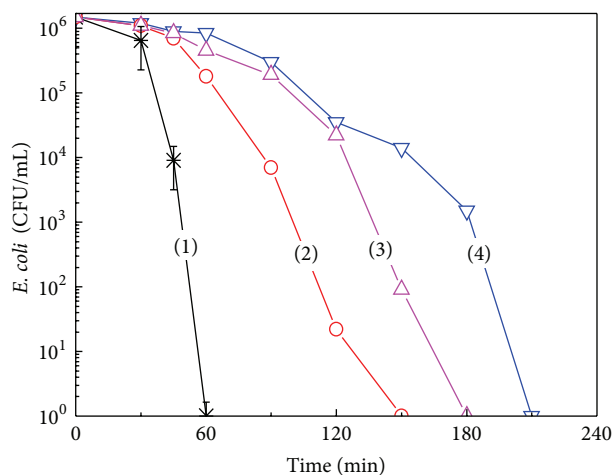
2.2. Surface XPS Analysis and ICP-MS of the Eluted Species during Bacterial Inactivation. An AXIS NOVA photoelectron spectrometer (Kratos Analytical, Manchester, UK) equipped with monochromatic AlK_α ($h\nu = 1486.6 \text{ eV}$) anode was



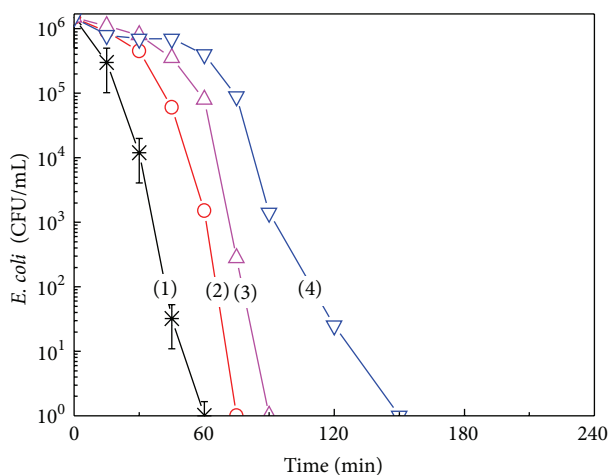
(a) TiO_2 sputtered for different times without RF-plasma pretreatment for (1) 8 min, (2) 10 min, (3) 5 min, and (4) polyethylene alone



(b) TiO_2 sputtered for 8 min with surface RF-plasma pretreatment at 1 torr for (1) 15 min, (2) 20 min, (3) 30 min, and (4) 5 min



(c) TiO_2 sputtered 8 min with RF air plasma pretreatment for (1) 15 min, (2) 20 min, (3) 30 min, and (4) 5 min



(d) TiO_2 sputtered 8 min with UVC pretreatment in air for (1) 20 min, (2) 15 min, (3) 10 min, and (4) 5 min

FIGURE 2: *E. coli* inactivation on TiO_2 sputtered on PE for 8 min irradiated with simulated solar light (52 mW/cm^2).

used during the study. The electrostatic charge effects on the samples were compensated by means of the low-energy electron source working in combination with a magnetic immersion lens. The carbon C1s line with position at 284.6 eV was used as a reference to correct for charging effects. The XPS spectra for the Ti-species were analyzed by means of spectra deconvolution software (CasaXPS-Vision 2, Kratos Analytical UK). The percentage surface atomic concentration of some elements was determined by fitting of the peak areas using known sensitivity factors [31]. Spectrum background was subtracted according to the Shirley subtraction GL(30) program attached to the Kratos unit [32, 33].

The polyethylene fabrics were pretreated in the cavity of the RF-plasma unit (Harrick Corp. 13.56 MHz, 100 W) at a pressure of 1 torr. Oxygen activated by RF-plasma reacts with the PE surface inducing functional PE-surface groups by (a) formation of oxygen containing hydrophilic surface groups and (b) scission of intermolecular PE-bonds due to localized heat segmenting the fibers [34]. PE was also functionalized by

UVC irradiation using the 185 nm emission wavelengths from a low-pressure mercury lamp (Ebara Corp. Tokyo, Japan). UVC activation, having a lower energy than the RF-plasma, does not lead to cationic or anionic oxygen species but only to atomic (O) and excited oxygen (O^*). The radiant energy at 185 nm provides energies above 241 nm equivalent to 495 kJ/mole or 6.70 eV, the energy required for the splitting of $\text{O}_2 \rightarrow 2\text{O}^*$ [12, 35].

Inductively coupled plasma spectrometry (ICP-MS) was used to determine the Ti since it is a sensitive analytical technique because of the low background and high ion transmission. The Finnigan ICPS used was used with a resolution of 1.2×10^5 cps/ppb, detection limit of 0.2 ng/L.

2.3. Diffuse Reflectance Spectroscopy (DRS), Electron Microscopy (TEM and HAADF), and XRD of Samples. Diffuse reflectance spectroscopy (DRS) was carried out using a Perkin Elmer Lambda 900 UV-VIS-NIR spectrometer provided for with a PELA-1000 accessory.

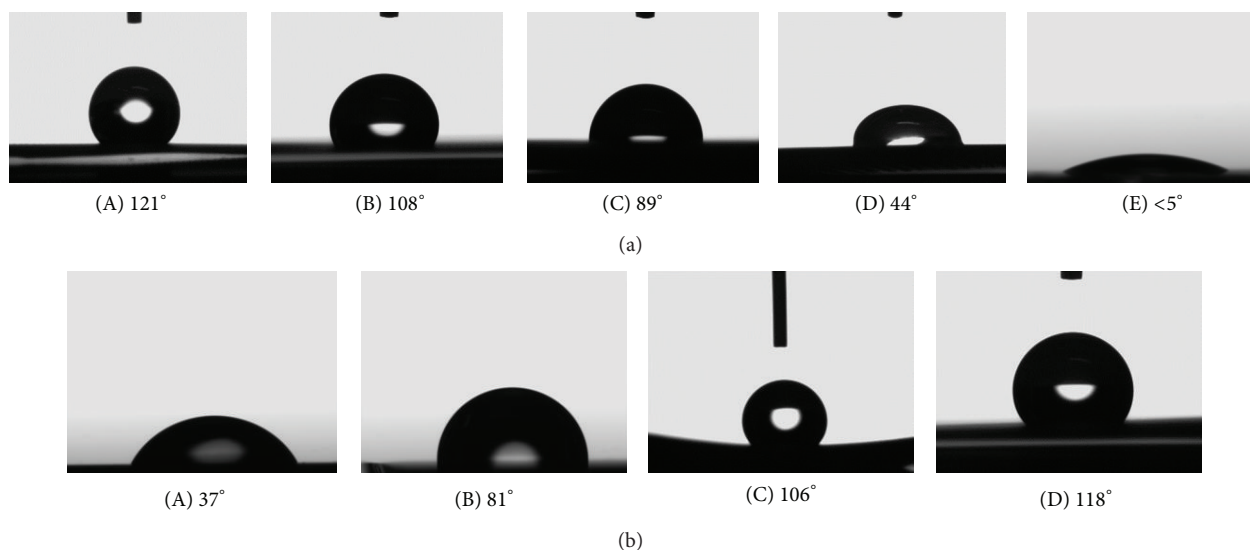


FIGURE 3: (a) Photoinduced superhydrophilicity followed by water droplet contact angle during light irradiation at times: (A) $t = 0$ min, (B) 15 min, (C) 30 min, (D) 45 min, and (E) 60 min. (b) Restoration of the hydrophilicity in the dark after times (A) 6 h, (B) 12 h, (C) 18 h, and (D) 24 h.

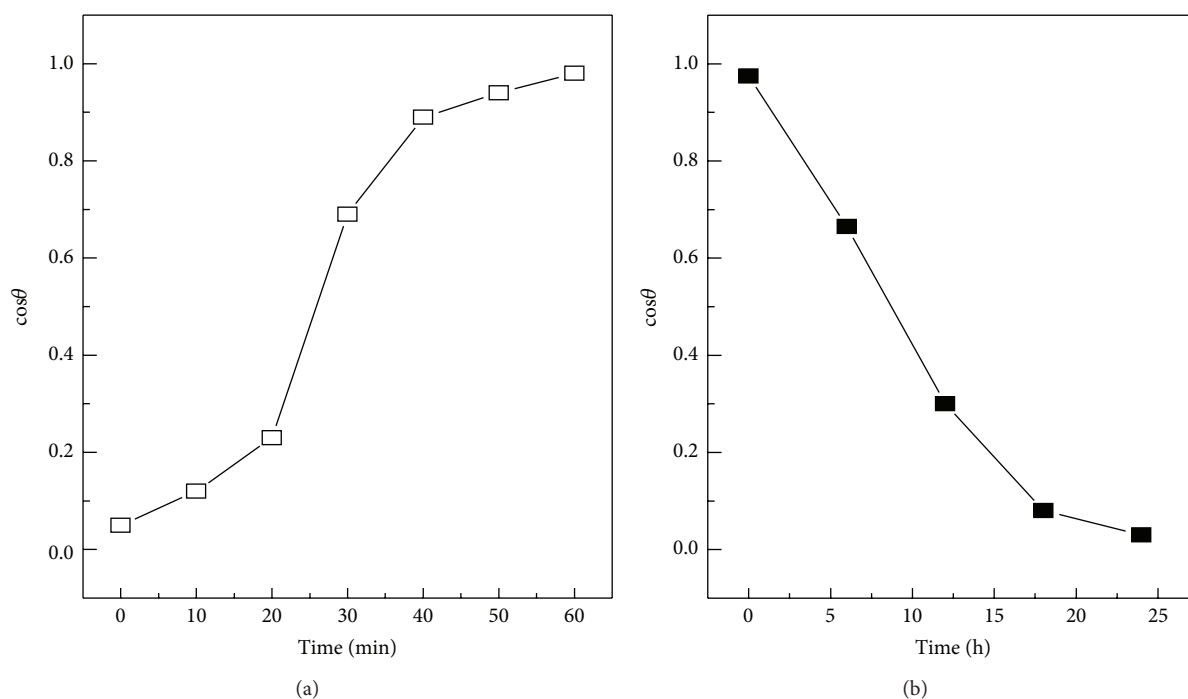


FIGURE 4: (a) Kinetics of the hydrophobic-hydrophilic transformation under solar simulated light and (b) kinetics of the dark reverse reaction towards the initial state for PE-TiO₂ (8 min) RF air plasma pretreated for 15 min.

The absorption of the samples was plotted in Kubelka-Munk (KM) arbitrary unit versus wavelength. Irradiation of the samples was carried out in a tubular cavity of a Suntest Heraeus solar simulator, Hanau, Germany, or in the cavity of a reactor provided with indoor actinic light (white light).

Transmission electron microscopy (TEM) was carried out in a Philips CM-12 (field emission gun, 300 kV, 0.17 nm

resolution) microscope at 120 kV and was used to measure grain size of the TiO₂. The textiles were embedded in epoxy resin 45359 Fluka and the fabrics were cross-sectioned with an ultramicrotome (Ultracut E) and at a knife angle of 35°. Crystal structures were characterized by X-ray diffraction (XRD) and recorded on an X'PertMPD PRO from PANalytical equipped with a secondary graphite (002) monochromator.

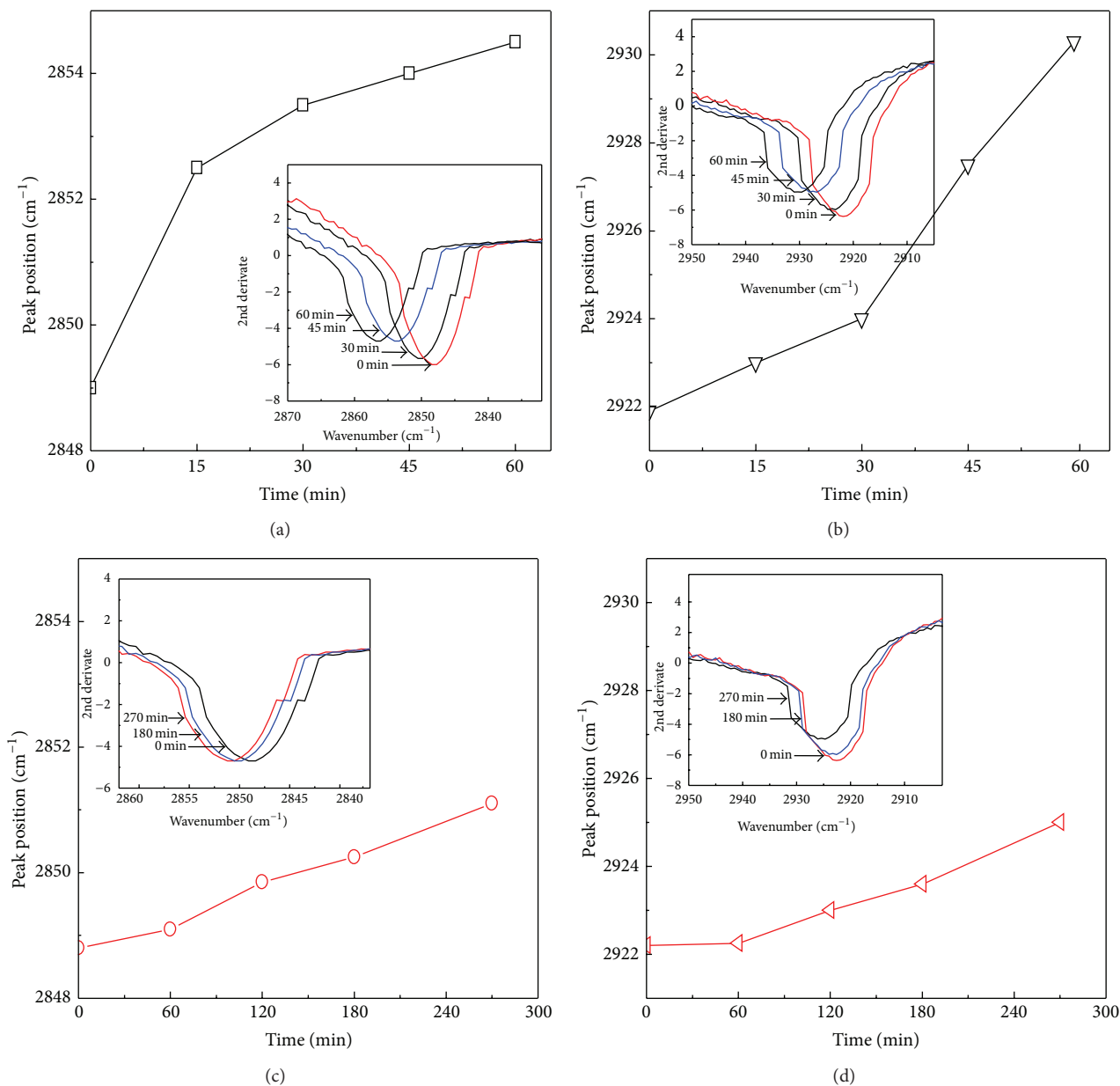


FIGURE 5: Shift of the stretching vibrations as a function of time detected by ATR-FTIR for the asymmetric $\nu_a(\text{CH}_2)$ vibrational bands and the symmetric $\nu_s(\text{CH}_2)$ vibrational bands for *E. coli* up to 60 min under solar simulated irradiation. (a) and (b) show the shifts of $\nu_a(\text{CH}_2)$ vibrational bands on PE-TiO₂ samples pretreated with RF air plasma for 15 min and then sputtered for 8 min. (c) and (d) show the IR shifts of $\nu_s(\text{CH}_2)$ vibrational bands on nonpretreated PE-sputtered for 8 min.

2.4. Contact Angle (CA) and ATR-IR Measurements. The hydrophilicity of the TiO₂ films was determined by the water droplet contact angle (CA). The CA of TiO₂ films on the substrate was determined by the sessile drop method on a DataPhysics OCA 35 unit. FTIR spectra were measured in a Portmann Instruments AG spectrophotometer equipped with a Specac attachment (the prism was a 45° one pass diamond crystal). Spectra were taken by 256 scans with a resolution of 2 cm⁻¹ in the range 900–4000 cm⁻¹. The position of the IR peaks was found by the second derivative of the spectra after Fourier deconvolution.

2.5. *E. coli* Loss of Viability Evaluation. The samples of *Escherichia coli* (*E. coli* K12) were obtained from the Deutsche Sammlung von Mikroorganismen und Zellkulturen GmbH (DSMZ) ATCC23716, Braunschweig, Germany, to test the antibacterial activity of the TiO₂-polyethylene and TiO₂-polyester films according to previous work reported by our laboratory [9]. Serial solutions were prepared in tryptone solution and the samples plated on agar Plate-Count-Agar (PCA, Merck, Germany). The bacterial counting data reported were obtained by the replicate of 3 experimental runs.

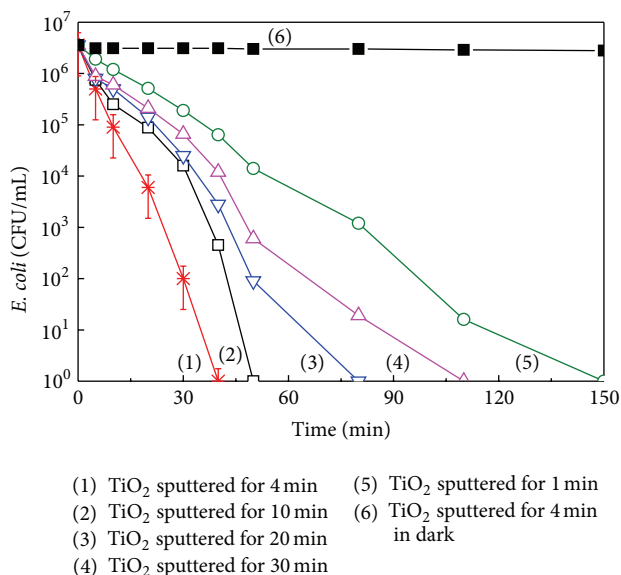


FIGURE 6: *E. coli* survival on TiO₂ HIPIMS-sputtered (5A) on polyester for different times in the dark and under solar simulated irradiation (50 mW/cm²).

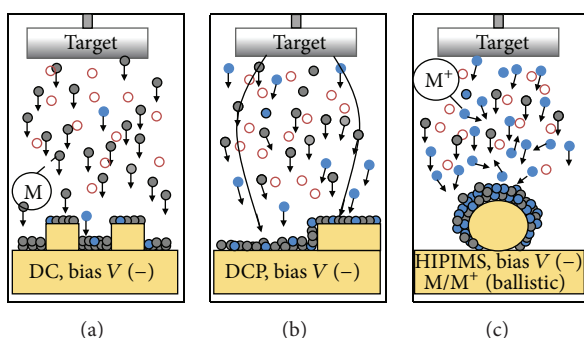


FIGURE 7: Scheme for the magnetron chamber induced M⁺ ionization by (a) DC, (b) DCP, and (c) HIPIMS sputtering of metals (M⁺) on 3D substrates showing the higher density ionization induced by HIPIMS.

To verify that no regrowth of *E. coli* occurs after the total inactivation observed in the first disinfection cycle, the samples were incubated for 24 hours at 37°C. After vortexing these samples in a 2 mL Eppendorf tube, the fabrics were placed on a PCA Petri dish, incubated overnight at 37°C to verify if still some bacteria remained adhered to the PE-TiO₂ surface. No bacterial colonies were observed. This indicates that the bacteria inoculated on the PE-TiO₂ surface remain in the Eppendorf tube. Then the bacterial 100 microliters suspensions were deposited on 3 Petri dishes to obtain replicates of the bacterial counting. No bacterial regrowth was observed.

Statistical analysis of the results was performed for the decrease of the bacterial CFU values reporting the standard deviation values for the runs showing the fastest bacterial

inactivation. The average values were compared by one-way analysis of variance and with the value of statistical significance.

3. Results and Discussion

3.1. TiO₂-PE Bactericide Thin Films Obtained by Sputtering Increasing *E. Coli* LPS Cell Wall Fluidity and Leading to Cell Lysis

3.1.1. *Support Choice for TiO₂ Deposition.* This first study addresses the sputtering of TiO₂ transparent, uniform, non-scattering films on polyethylene (PE). Sol-gel commercial methods are used to prepare TiO₂ thin films on heat resistant substrates. But on nonthermal resistant substrates the thickness of the TiO₂ films is not reproducible and they are not mechanically stable [6–10, 15].

Polyethylene (PE) is a low cost and is widely available material. It is chemically inert, mechanically stable and flexible, and UV-resistant and does not oxidize in air under sunlight. In addition, the hydrophobic nature of PE allows the deposition of predominantly hydrophobic pathogens. Bacterial hydrophobic outer cell walls will adhere preferentially on hydrophobic surfaces promoting bacterial inactivation. PE-TiO₂ films intend to overcome the use of TiO₂ powders or suspensions for bacterial disinfection. Suspensions of TiO₂ need a long-settlement time after each disinfection cycle being applied with significant loss of catalyst mass [6, 7]. The PE-TiO₂ transparent films are designed to increase the quantum yield of the TiO₂ radical species in addition to the direct bactericide action of sunlight [11, 14]. TiO₂ sputtering does not lead to the deposition of enough TiO₂ on the PE due to the low binding capacity of the PE surface. RF-plasma pretreatment induces oxygen negatively charged functional groups, for example, carboxylic, percarboxylic, epoxide, and peroxide groups by the atomic O, excited O, and anionic and cationic O generated in the RF-plasma chamber [12–14]. The PE functionalized negative sites bind the slightly positive sputtered Ti⁴⁺ (TiO₂) through electrostatic attraction involving chelation/complexation [34, 35]. The TiO₂ was sputtered immediately after the RF-plasma pretreatment due to the short lifetimes of the surface polar hydrophilic surface sites.

3.1.2. *PE Pretreatment, TiO₂ Surface Sputtered PE, Sample Absorption, and TiO₂ Crystalline Phases.* The amount of TiO₂ on the pretreated PE fabrics was determined by X-ray fluorescence XRF using the nonpretreated fabric as the blank. For the sample pretreated in air for 15 min by RF plasma and sputtered for 8 min, a TiO₂ thickness of ~58 nm was attained on PE equivalent to 290 layers. Taking one layer with 10¹⁵ atoms/cm² and the thickness of one layer as 0.2 nm, the rate of TiO₂ deposition was of 6 × 10¹⁴ atoms/cm².s. Self-cleaning TiO₂ films up to 10 microns thick have been reported [1–5], but in the case of antibacterial coatings TiO₂ thicknesses of 1 nm–20 nm have been reported to be effective [3, 6, 7]. TiO₂ films DC sputtered for 8 min consist

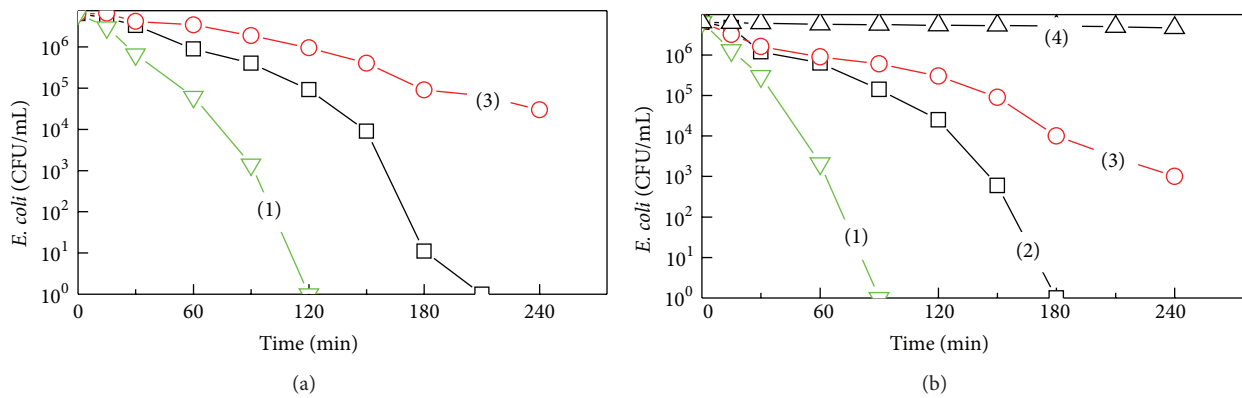


FIGURE 8: *E. coli* inactivation under solar simulated light for (1) $\text{TiO}_2/\text{In}_2\text{O}_3$ (sputtered for 10 min/10 s), (2) TiO_2 (sputtered for 10 min), (3) In_2O_3 (sputtered for 10 s) samples, respectively, and (4) a bare polyester sample, at light intensities: (a) $30 \text{ mW}/\text{cm}^2$ and (b) $50 \text{ mW}/\text{cm}^2$.

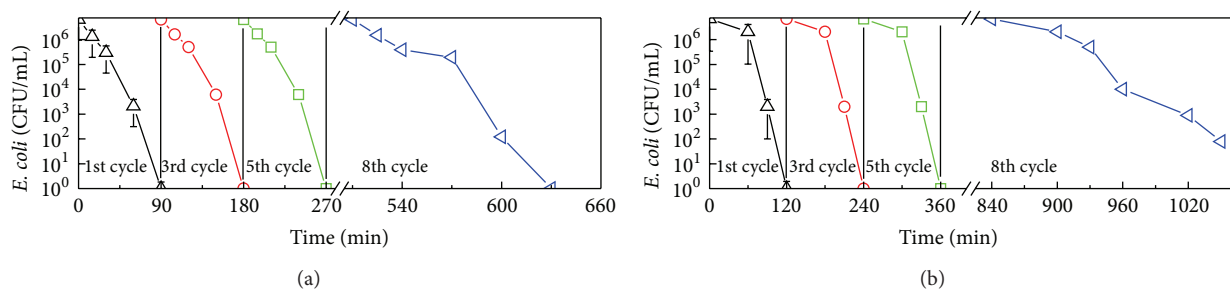


FIGURE 9: *E. coli* inactivation recycling experiments on $\text{TiO}_2/\text{In}_2\text{O}_3$ sputtered for 10 min/10 s on polyester under irradiation by: (a) Osram Lumilux T8-L 18 W ($4.0 \text{ mW}/\text{cm}^2$, 360 to 800 nm) and (b) Suntest solar simulator $50 \text{ mW}/\text{cm}^2$.

of nanoparticles 10–30 nm in size [36] and the films were reproducible.

The RF-plasma induced functional groups only on the PE topmost layers since no color changes occurred destroying the PE structure indicative of PE-degradation [37].

The DRS spectra of the PE- TiO_2 films are shown in Figure 1 for samples pretreated by RF and UVC light. Sputtering for 1 to 3 min leads to transparent TiO_2 films with no significant absorbance and very low antibacterial activity. A decrease of ~5% or more in optical transmittance has been reported for RF-plasma pretreated PE [38]. The decrease in transmittance for the sputtered films in Figure 1 was due to the inherent high refractive index of TiO_2 .

The TiO_2 crystal phases on PE show by XRD a high anatase (A) peak at $2\theta = 21.5^\circ$ [34] for a PE- TiO_2 with and without RF-plasma pretreatment. But XRD peaks of rutile (R) at temperatures $\leq 130^\circ\text{C}$ found in the DC-magnetron chamber were also observed. The generation of rutile at low temperatures is due to the structure forming function of the PE film on the TiO_2 as reported for polyamide and other sputtered TiO_2 textiles [12].

3.1.3. Antibacterial Kinetics Evaluation and Sample Recycling. Figure 2 shows *E. coli* inactivation on PE- TiO_2 films under simulated solar light with an integrated light dose of $52 \text{ mW}/\text{cm}^2$. The fastest bacterial inactivation was found

for pretreated PE samples TiO_2 sputtered for 8 min in Figure 2(a). Bacterial inactivation on PE- TiO_2 samples is presented in Figure 2 for RF-pretreated PE for different times. No significant bacterial inactivation was observed for bacteria on uncoated PE (Figure 2(a), trace (4)). Only trace (1) was subjected to statistical analyses since it describes the results for the most favorable kinetics and presents the highest amount of TiO_2 sites in exposed positions to interact with bacteria [39]. PE- TiO_2 sputtered samples for 1 up to 5 min were not loaded with sufficient TiO_2 to drive a fast bacterial inactivation. The Ti-loading on PE- TiO_2 was determined by XRF for sputtering times of 1, 3, and 5 min and the values found were, respectively, 0.009, 0.019, and 0.031 TiO_2 wt%/wt PE.

Samples sputtered for times >8 min in Figure 2(b) led to layer thickness >45 nm. This thickness leads to charge bulk inward diffusion decreasing the charge transfer between the PE- TiO_2 and bacteria [40]. TiO_2 sputtering for 8 min led to a TiO_2 loading with the most suitable thickness for the charge diffusion able to reach bacteria. Figure 2(c), trace (1) shows the fastest bacterial inactivation for PE- TiO_2 films. No significant bacterial inactivation was observed for bacteria on PE in the dark.

To verify that no regrowth of *E. coli* occurs after the first bacterial inactivation cycle, the PE- TiO_2 film was incubated

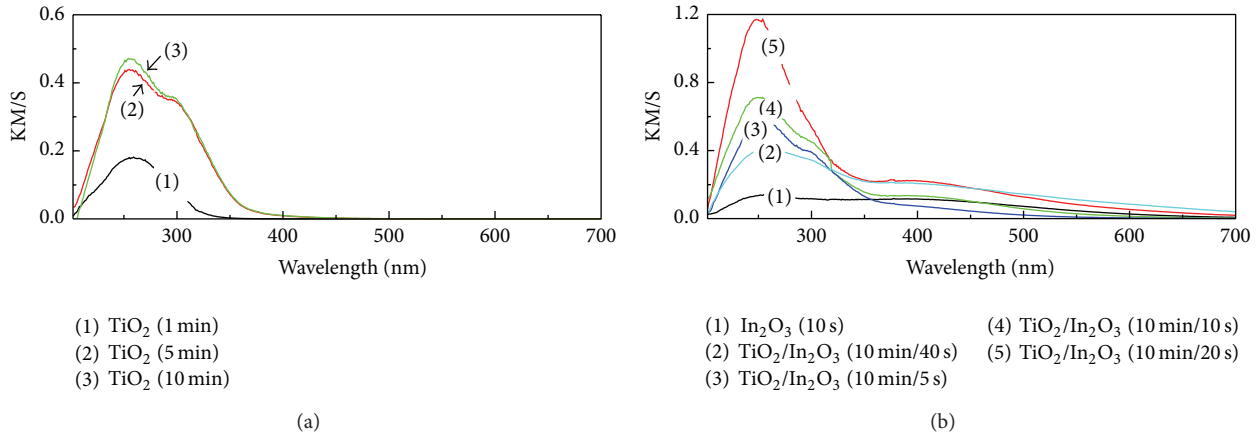


FIGURE 10: Diffuse reflectance spectra (DRS) of TiO₂ and TiO₂/In₂O₃ samples in Kubelka-Munk units: (a) TiO₂ 1 min, TiO₂ 5 min, and TiO₂ 10 min. (b) TiO₂ 10 min/In₂O₃ 5 s, TiO₂ 10 min/In₂O₃ 10 s, TiO₂ 10 min/In₂O₃ 20 s, and TiO₂ 10 min/In₂O₃ 40 s, In₂O₃ 10 s.

on an agar Petri dish for 24 hours at 37°C. No bacterial regrowth was observed meaning that there was no bacteria adhered to the surface after the inactivation cycle.

The bacterial inactivation by PE-TiO₂ samples sputtered for 8 min and pretreated with RF-plasma in air for 15 min was investigated up to the 6th cycle. The recycling of the samples showed stable inactivation kinetics up to the 5th-cycle; then the recycling kinetics became slower by ~20%. After each cycle, the samples were washed with distilled water and dried. Then, the samples were kept in an oven at 60°C to avoid bacterial contamination. After washing PE-TiO₂ the samples were left standing for 24 h before to regain the initial sample hydrophobicity. This aspect will be discussed below in Section 3.1.4 when discussing the hydrophilic-hydrophobic transformation on PE-TiO₂ in the dark and shown in Figures 3(a) and 3(b).

3.1.4. Contact Angle (CA) and Hydrophobic Reversible Photoswitching. Figure 3(a) presents the hydrophobic to hydrophilic transformation occurring on the PE-TiO₂ sample induced by simulated solar light. A decrease of the CA from 121° to less than 5° within 60 min is shown in Figure 3(a) (traces (A)–(E)) concomitant with the time of bacterial inactivation. The recovery from the PE-TiO₂ superhydrophilic surface to a hydrophobic initial surface proceeded within 24 hours in the dark as shown in Figure 3(b).

The transformation of the initial hydrophobic TiO₂ under light irradiation involves the dissociative chemisorption of water on the PE-TiO₂ generating Ti-OH groups [41, 42]. Under light irradiation, the PE-TiO₂ generates electrons (e⁻) and holes (h⁺) producing OH[•] and O₂⁻ radicals. The photogenerated h⁺ are the precursors of OH[•]. The structural changes in the TiO₂ surface due to hydrophilicity are associated with the generation of these radicals. This process does not require high quantum efficiency in comparison to the *E. coli* photocatalytic oxidation. A second mechanism has been suggested for the hydrophobic to hydrophilic transformation

and would be due to TiO₂ generated charges leading to oxygen vacancies reducing Ti⁴⁺ to Ti³⁺ [43].

Figure 3(b) shows the hydrophilic to hydrophobic reversible transformation in the dark reinstating the initial TiO₂ hydrophobicity within 24 hours. The hydrophilic samples were kept in the dark and the contact angles (CA) were measured at preselected times to follow the back reaction to the initial hydrophobic state. This second process involves the destruction of airborne bacteria or hydrocarbons adsorbed on the PE-TiO₂ surface along TiO₂ surface dehydration and the back conversion of Ti³⁺/Ti⁴⁺ [42].

Figure 4(a) illustrates the rate of photoinduced hydrophilicity and Figure 4(b) the restoration rate of the hydrophobicity in the dark as a function of “cos θ”. According to Young’s theory the “cos θ” of a liquid droplet on a solid surface is a function of the interfacial energy between the solid and the liquid. The rate of the hydrophobic to hydrophilic conversion and for the reverse reaction in Figures 4(a) and 4(b) was 0.277 min⁻¹ and was 8.71 × 10⁻³ min⁻¹, respectively. These rates were calculated by integrating “cos θ” in Young’s equation (1).

The contact angle (CA) conventionally measures the angle where the liquid meets the solid quantifying the wettability of a solid surface via the Young equation. The Young equation (1) involves solid-vapor, liquid-vapor, and solid-liquid interfacial energies. The solid-vapor interfacial energy is denoted by γ_{SG}, the solid-liquid interfacial energy by γ_{SL}, and the liquid-vapor interfacial energy (i.e., the surface tension) by γ_{LG}; then the equilibrium contact angle θ_C is determined from these quantities by Young’s equation:

$$0 = \gamma_{SG} - \gamma_{SL} - \gamma_{LG} \cos \theta_C. \quad (1)$$

Upon illumination the surface TiO₂ energy increases since the TiO₂ surface is transformed into a metastable state as shown in (2) decreasing the initial contact angle of 121° (Figure 3(a)) to a value of <5° after 60 min irradiation (Figure 3(b)). Equation (2) shows the TiOH metastable hydrophilic intermediate induced under light:

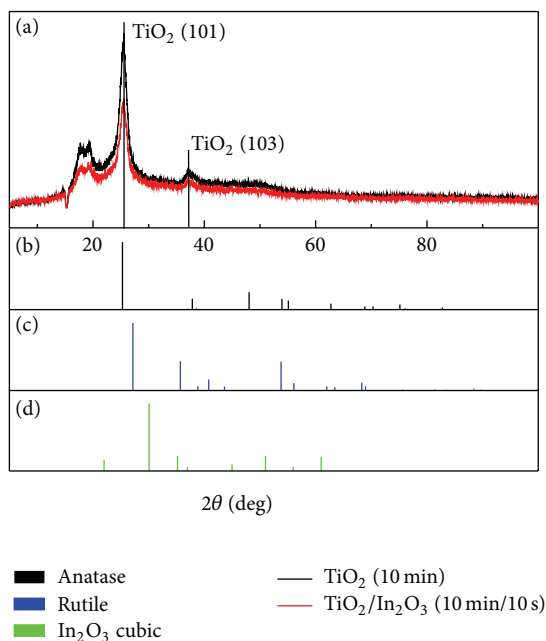
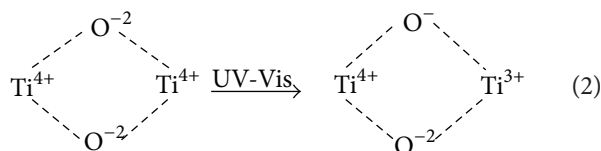


FIGURE 11: XRD diffraction data for (1) TiO_2 sputtered for 10 min on polyester and (2) TiO_2 10 min / In_2O_3 10 s sputtered on polyester: (a) diffraction patterns of anatase (b), rutile (c), and (d) cubic In_2O_3 .



The hydrophobic properties of the PE- TiO_2 surface are important in antibacterial films. *E. coli* and *Staphylococcus aureus* present a preferential adhesion to hydrophilic surfaces [44]. Bacteria with hydrophobic surface properties like *S. epidermidis* adhere preferentially to hydrophobic surfaces [45]. Hydrophobic bacteria adhere to a variety of surfaces forming biofilms to a greater extent than hydrophilic bacteria [46]. Recently, R. Amal recently has reported the reversible photoswitching behavior under light by TiO_2/Ag nanoparticles [47, 48]. This study shows that UV-A irradiation of brownish Ag/TiO_2 changed the surface Ag_2O to violet black, the characteristic color of Ag-plasmon. Nano-Ag particles are responsive to visible light due to the enhanced surface plasmon resonance (SPR) absorption band at ~ 550 nm. As a result of visible light excitation a reverse electron flow from Ag^0 to the TiO_2 cb occurs along the oxidation of metallic Ag^0 back to Ag_2O . A reversible antimicrobial photoswitching of nano-Ag/ TiO_2 particles was reported in this study when irradiating the Ag-nanoparticles in two different wavelength regions [48].

3.1.5. FTIR Analysis and Bacterial Inactivation on PE- TiO_2 . FTIR spectroscopy is used in the present study to monitor the changes in the structure/dynamics in the *E. coli* lipopolysaccharide (LPS) bilayer induced by PE- TiO_2 under solar simulated light. LPS amphiphiles constitute the outer

cell wall of *E. coli* and consist of LPS units. The LPS are made up of fluid chains [49]. (CH_2) - and (CH_3) -groups make up 70% of the lipopolysaccharide (LPS), phosphatidylethanolcholine (PE), and peptidoglycan (PGN), the main groups making the *E. coli* cell envelope [49, 50].

The characteristic bands of the methylene ($-\text{CH}_2$) stretching vibrations in the 2800 – 2900 cm^{-1} spectral region are shown in Figure 5. Figure 5(a) shows the shift of the asymmetric methylene stretching vibrations at $\nu_a(\text{CH}_2)$ 2922.2 cm^{-1} and of the symmetric stretching vibrations of $\nu_s(\text{CH}_2)$ at 2849.2 cm^{-1} for RF-plasma pretreated samples for 15 min and sputtered for 8 min and then irradiated up to 60 min. The shifts in the peaks for RF-plasma pretreated PE- TiO_2 samples in Figures 5(a) and 5(b) are seen to be more important compared to the nonpretreated samples shown in Figures 5(c) and 5(d). This is due to the lower amount of TiO_2 on the nonpretreated PE leading to longer bacteria inactivation times. The shifts presented in Figure 5 reflect the structural/conformation changes in LPS during lipid peroxidation involving the production of peroxides, alcohols, and carboxyl type functionalities associated to the bacterial lysis and bacterial dead.

The decrease in the amplitude observed for the stretching vibrations in the ATR-IR-spectra in Figures 5(a)–5(d) was due to isolated double bonds in the LPS. The discontinuous shifts towards the blue in Figures 5(a) and 5(b) suggest an increased mobility of the LPS units in the LPS chain-packing [49]. The increased disorder modifies the frequencies of the $-\text{CH}_2$ symmetric and antisymmetric bands, shifting the peak positions during the irradiation time [51]. Figure 2(c), trace (1) shows that *E. coli* inactivation is complete within 60 min on PE- TiO_2 and this time coincides with the time in which the LPS stretching vibrations attain the highest fluidity. This time coincides with the time to attain the intermolecular distances leading to $-\text{CH}_2$ scission (60 min) [52–54].

3.1.6. TiO_2 Films Sputtered by HIPIMS Leading to Accelerated *E. Coli*. Figure 6 shows the bacterial inactivation kinetics by the HIPIMS TiO_2 sputtered samples [28]. As shown in Figure 6, no bacterial inactivation takes place in the dark, but the bacterial inactivation becomes faster for HIPIMS sputtering times between 1 min (trace (5)) and 4 min (trace (2)). Longer deposition times between 10 and 30 min did not accelerate the loss of viability kinetics due to the fact that an increased TiO_2 thickness > 12 nm sputtered within 4 min leads to (a) bulk inward diffusion of the charge carriers generated on TiO_2 under light leading to highly oxidative radicals [6–10] and (b) longer sputtering times facilitate the TiO_2 interparticle growth decreasing the TiO_2 contact surface with bacteria.

The bacterial inactivation time shown in Figure 6 for polyester surface sputtered by HIPIMS is faster compared to DC and DCP TiO_2 -polyester sputtered surfaces [36].

3.1.7. DCP and HIPIMS Sputtering of Samples, Electronic Density, and Voltage Considerations. Figure 7, left hand side presents a scheme for the DC sputtering and in the middle section Figure 7 shows the sputtering of DCP proceeding

with a higher ionization of Ti at higher e-densities ($\sim 10^{16-17} \text{ e}^-/\text{m}^3$) [55]. The HIPIMS with 5A and consequently a much higher energy than the HIPIMS pulses increases the ionization percentage $\text{Ti}^0 \rightarrow \text{Ti}^{3+}/\text{Ti}^{4+}$ with a concomitant increase in the e-densities ($\sim 10^{18-19} \text{ e}^-/\text{m}^3$).

This increased arrival energy of the Ti-ions on the substrate allows the alignment of the Ti-ions on the polyester irregular (rugous) surface enabling a uniform coverage of the 3D polyester, oximeters, and pressure blood measuring devices as usually used in medical facilities. These artifacts are sources of infections, since they are not TiO_2 coated. The HIPIMS sputtering shown on the right hand side in Figure 7 allows the uniform sputtering of objects with complex 3D geometry due to their increased e-density interacting more favorably with the negatively biased substrate compared to the less dense production of ionized species shown in Figures 7(a) and 7(b) [29, 55, 56].

3.2. Uniform TiO_2 -Doped In_2O_3 Films Increasing the Bacterial Inactivation Kinetics with respect to TiO_2 -Films under Low Intensity Solar Simulated Light

3.2.1. TiO_2 Sputtered on Pretreated PE. This study shows that the surface modification of TiO_2 by doping with In_2O_3 is an effective route to increase the TiO_2 absorption into the visible region. A photoinduced interfacial charge transfer (IFCT) between TiO_2 and In_2O_3 takes place and couples the charge generation/separation between these two oxides. In_2O_3 has an absorption band in the visible between 400 nm and 500 nm [57].

The TiO_2 and TiO_2 - In_2O_3 thin films were deposited onto polyester in the magnetron chamber by sputtering Ti by DC in a reactive O_2 atmosphere followed by DCP sputtering of In, in the presence of mixture of Ar and O_2 gases. The total working pressure $P = (P_{\text{Ar}} + P_{\text{O}_2})$ was fixed at 0.5 Pa and the ratio $P_{\text{O}_2}/P_{\text{total}} = 4.5\%$. The sputtering current on the Ti target was 280 mA providing a power of 120 W ($U = -450 \text{ V}$) and a current density of $12.7 \text{ mA}/\text{cm}^2$. Pulsed magnetron sputtering (DCP) was used to sputter the In_2O_3 and was operated at 50 kHz with 15% reversed voltage. The sputtering power was fixed at 50 W providing a negative voltage of -500 V and a power of 140 W.

3.2.2. Evaluation of the Bacterial Inactivation of *E. coli* in the Dark and under Light. The counting of the bacterial inactivation of *E. coli* was performed as described above in Section 2.4 [28, 36]. An actinic irradiation lamp Osram Lumilux T8-L 18 W ($4.0 \text{ mW}/\text{cm}^2$) was used in Figure 8 as a source of white light. This light is used for the indoors lightning in health facilities. The solar simulator (Heraeus, Hanau, Germany) emitting between 200 and 800 nm from a 100 W Xe-light resembling the solar spectrum and set at $50 \text{ mW}/\text{cm}^2$. The value of $50 \text{ mW}/\text{cm}^2$ is the average light dose reaching central European countries. Figure 8 shows the inactivation of *E. coli* by TiO_2 , TiO_2 - In_2O_3 , and In_2O_3 samples.

A synergic interaction of TiO_2 is required to lead to fast bacterial inactivation in Figure 8(a), trace (1). Figure 8(b), trace (4) shows that no bacterial inactivation was possible under light on bare polyester. Figure 8(a) reports the effect of the light intensity on the amount of charges in the coupled semiconductors at $30 \text{ mW}/\text{cm}^2$ and $50 \text{ mW}/\text{cm}^2$. A higher light intensity increases the amount of semiconductor charges interacting with bacteria leading to a faster bacterial inactivation. The accelerated bacterial inactivation by the TiO_2 - In_2O_3 photocatalysts compared to bare TiO_2 samples is favoured by the electrostatic attraction existing between the positive charged Ti and the negative *E. coli* cell wall at pH 6-7. The *E. coli* is negatively charged between pH 3-9 due to the excess of carboxylic groups compared to the amide I and amide II cell wall positively charged groups [3, 58]. The TiO_2 bacterial inactivation under light has been widely reported and will not be discussed in this study [6-10].

Figure 9 shows repetitive disinfection cycles by a TiO_2 - In_2O_3 sputtered for 10 min from a TiO_2 target and 10 s from an In target in a reactive O_2 atmosphere, up to the 5th cycle. The 8th cycle shows a loss of bacterial inactivation kinetics when actinic light was used in Figure 9(a) and when a solar simulator with a dose of $50 \text{ mW}/\text{cm}^2$ was applied. The slower kinetics shown in Figure 9(b) in the last cycle was due possibly to the leaching of In and Ti-nanoparticles detected by ICP-MS (data not shown).

3.2.3. Diffuse Reflectance Spectroscopy (DRS) and X-Ray Diffraction (XRD) Investigation of TiO_2 and TiO_2 - In_2O_3 Films.

Figure 10 shows the UV-Vis reflectance spectra of TiO_2 sputtered as a function of time. The Kubelka-Munk (KM/S) relations convert reflectance measurements into absorption spectra units. K and S are the absorption and scattering coefficients, respectively, of TiO_2 in Figure 10(a). The KM/S values for the samples were found proportional to the TiO_2 sputtering time. The faster bacterial inactivation induced by TiO_2 - In_2O_3 and shown in Figure 8 suggests an electron transfer from In_2O_3 to TiO_2 .

Figure 10(b) shows a progressive increase in optical absorption (KM/S spectra) in the region 350 nm. Samples sputtered with In_2O_3 for 5-20 s show lower absorption intensities. Figure 10(b) shows a weak absorption band from 400 to 500 nm, attributed to the interfacial charge transfer (IFCT) from the TiO_2 to In_2O_3 . The weak absorption between 500 and 600 nm is due to the In_2O_3 interband indirect transitions at potential levels 2.09 eV [25]. These electronic transitions occur from the In_2O_3 valence band to two levels near the conduction band $\geq 2 \text{ eV}$ [59]. The TiO_2 - In_2O_3 transition seems to originate from the In_2O_3 ($\text{In}5s5p$ orbital) to the conduction band of TiO_2 . The light green color In_2O_3 samples with band-gap of 2.5-2.8 eV (absorption edge ~ 470 -500 nm) became darker at longer sputtering times [60, 61].

Figure 11 shows the TiO_2 XRD of TiO_2 and $\text{In}_2\text{O}_3/\text{TiO}_2$ films, respectively. Figure 11 presents the XRD diffraction for the TiO_2 DC sputtered on polyester for 10 min. The intense anatase peak at 24.6° is due to the presence of anatase. No specific signal due to In_2O_3 was detected due to its very

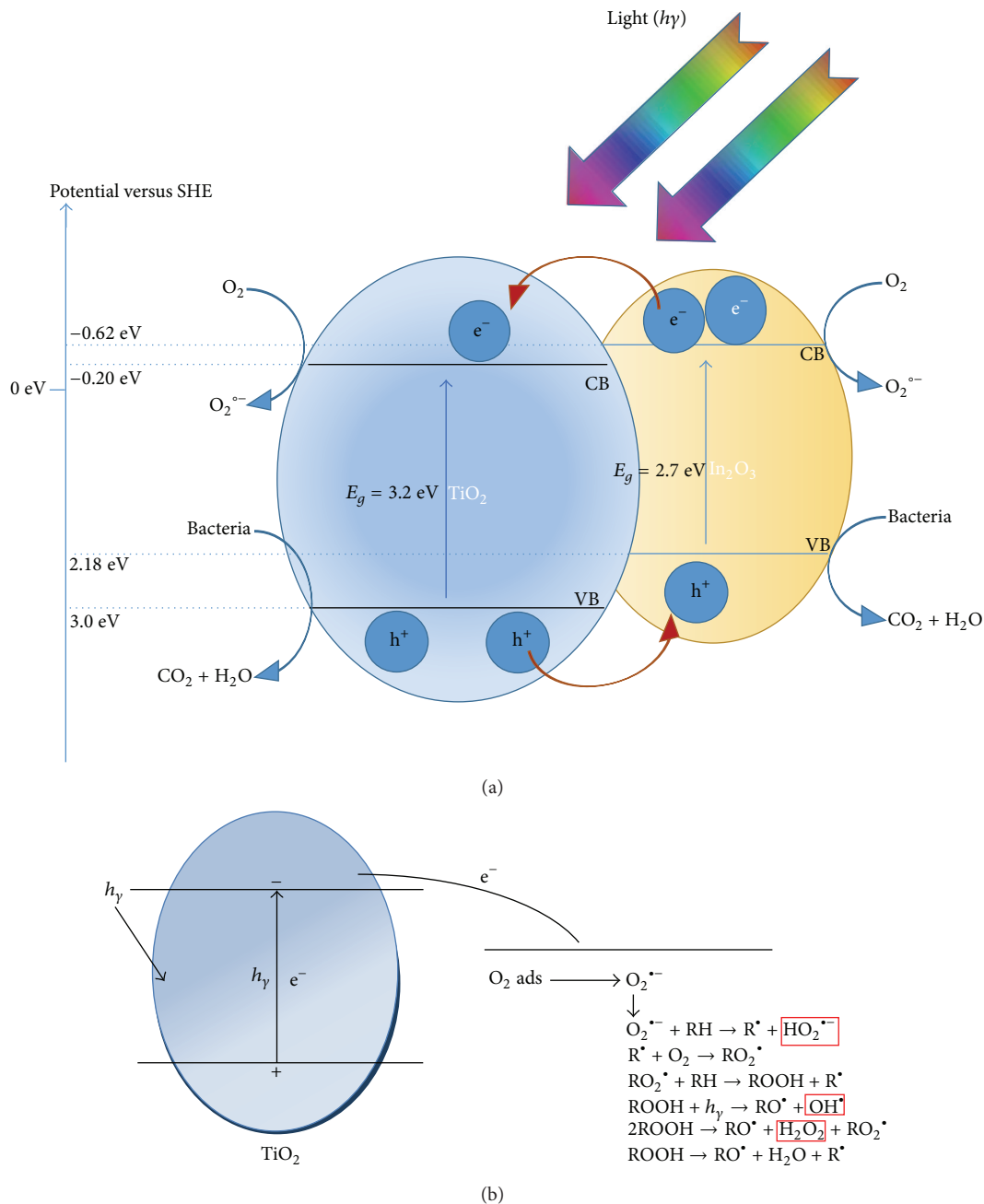


FIGURE 12: (a) Scheme of the charge injection during the interfacial charge transfer (IFCT) between In_2O_3 and TiO_2 under simulated sunlight. (b) Radical(s) reaction generated from O_2 reduction on TiO_2 (R: bacteria degradation or species produced during the bacterial degradation).

low loading (<0.2%). Only a slight decrease in intensity of the 24.6° (101) anatase peak was observed in the $\text{In}_2\text{O}_3/\text{TiO}_2$ samples. No modification in the TiO_2 diffraction peaks due to In_2O_3 was observed, suggesting that no lattice modification due to In-doping takes place in the TiO_2 network.

3.2.4. Interfacial Charge Transfer Mechanism (IFCT) in TiO_2 - In_2O_3 Composite Films. Coupling TiO_2 - In_2O_3 induced a significant increase in the photocatalytic activity compared to TiO_2 alone and In_2O_3 as shown in Figure 8. This significant

increase can be rationalized by the relative positions of the conduction band (cb) and valence band (vb) in In_2O_3 and TiO_2 . The cb of In_2O_3 at -0.62 versus NHE [60, 61] transfers the cb electrons to TiO_2 (cb at 0.2 eV versus NHE for anatase). The UV component of sunlight generates TiO_2 holes able to transfer to In_2O_3 vb as shown in Figure 12(a). The subsequent spatial separation of photogenerated charge carriers and the e^- and h^+ injection limit the e^-/h^+ recombination on TiO_2 .

The highly dispersed In_2O_3 on the TiO_2 layers builds a Schottky barrier at the $\text{TiO}_2/\text{In}_2\text{O}_3$ interface. This precludes partly the recombination of electrons and holes in TiO_2 . The

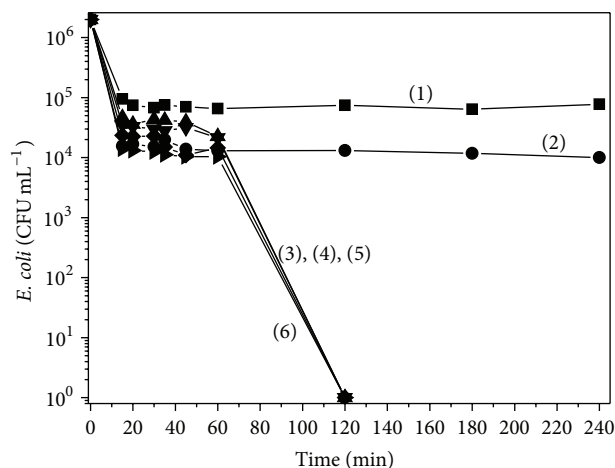


FIGURE 13: Loss of bacterial viability in the dark mediated by TiO₂-polyester (HT) prepared samples with different TiO₂ loadings: (1) polyester alone, (2) 0.05%, (3) 0.1%, (4) 0.5%, (5) 1%, and (6) 5%.

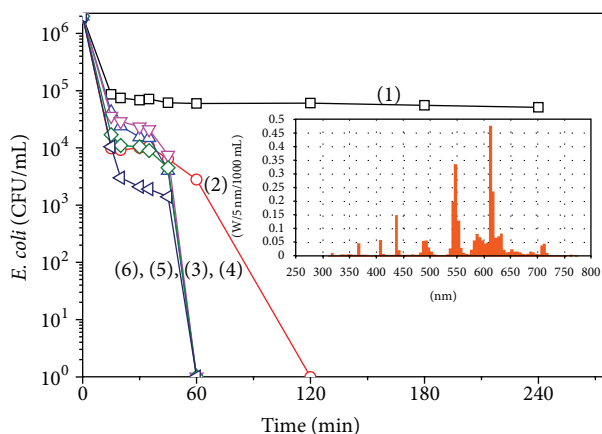


FIGURE 14: Loss of bacterial viability of *E. coli* under Osram Lumilux 18 W/827 irradiation mediated by TiO₂-polyester HT prepared samples with a TiO₂ loading: (1) polyester alone, (2) 0.05% (3) 0.1% (4) 0.5%, (5) 1%, and (6) 5%.

scheme in Figure 12(a) suggests an IFCT to take place in the TiO₂-In₂O₃ assuming that the generated charges have a sufficient lifetime to diffuse to the photocatalyst surface inactivating bacteria. The TiO₂ is the main photocatalyst and the In₂O₃ acts as a visible light sensitizer. In Figure 12(a) a detrimental effect may be due to the cross interparticle recombination of the e⁻_{cb} of TiO₂ with the h⁺_{vb} of In₂O₃ [62].

Figure 12(b) shows schematically the e⁻_{cb} in the TiO₂ and In₂O₃ particles reacting with the adsorbed O₂ on the TiO₂ surface to yield O₂^{-•} radical anion and subsequently other highly oxidative protonated radicals active in the bacterial inactivation.

3.3. New Evidence for the Inactivation of TiO₂ Films with Bacteria in the Dark. This study addresses the design, preparation, and bacterial counting of the bacterial inactivation kinetics and characterization of TiO₂-polyester surfaces

inducing cell wall damage with concomitant loss of bacterial viability in the dark. In 1985, Matsunaga et al., [63] reported that TiO₂ suspensions inactivate bacteria. After Matsunaga many studies have reported on the TiO₂ photocatalytic bacterial cell wall damage [64–66]. The bacterial inactivation by agents permeating into the cell structure has also been widely reported [5, 6, 67]. Few articles have reported cell wall damages by the photocatalysis by electron microscopy (EM) [5]. *P. aeruginosa* outer cell wall damages due to TiO₂ photocatalysis have been reported recently by P. Amezaga-Madrid et al. [68–74]. The TiO₂ interaction with the bacteria was reported to cause damages/disorganization in the cell wall morphology modifying its permeability and the capacity to regulate the outer layers osmotic pressures. The importance of the present study on antimicrobial surfaces relates to the fact that bacteria survive for long times in hospital facilities increasingly leading to hospital acquired infections (HAI). Precluding the infectious biofilm formation by the TiO₂-polyester surfaces in the dark is an effective way to reduce/suppress infections as will be reported in this study.

3.3.1. Preparation of TiO₂-Polyester by the Hydrothermal Route and *E. coli* Loss of Viability in the Dark and under White Light. The TiO₂ on the polyester deposition by the hydrothermal route (HT) was carried out as follows: titanium tetraisopropoxide (TTIP) Sigma Aldrich p.a. was dissolved in isopropanol in a 1:3 volume ratio (1:3 molar ratio). This solution was poured into a beaker with 50 mL of 0.1 M HNO₃. The polyester samples 6 × 4 cm were immersed into the acid TiO₂ precursor suspension and heated under stirring in a reflux condenser for 2 hours at 80°C. The polyester fabric was removed from the suspension, rinsed with demineralized water, and treated in ultrasound bath for 2 min to remove unbound TiO₂ particles. The last operation was repeated three times and the TiO₂-polyester fabric were subsequently dried for 2 hours at 70°C in air [75]. The inactivation of *Escherichia coli* (*E. coli* K12) on TiO₂ polyester samples was evaluated according to Section 2.4.

In Figure 12 no significant bacterial loss of viability was observed for bacteria on uncoated samples (Figure 13, trace (1)). A loading of 0.05% TiO₂ on the TiO₂-polyester in Figure 13, trace (2) did not contain enough TiO₂ to induce bacteria loss of viability. TiO₂ loadings between 0.1% and 5% led to similar bacterial loss of viability within 120 min. This indicates that the number of cells capable of forming colonies in contact with the cell wall surface attained a stable value for TiO₂-polyester surfaces loaded between 0.1% and 5.0%.

Figure 14 shows the loss of bacterial viability under light irradiation within 60 min for TiO₂-polyester at loadings above TiO₂ 0.1%. The insert in Figure 14 shows the spectral emission of the actinic Osram Lumilux 18 W/827 light used with a dose of 4.0 mW/cm². The mechanism leading to bacterial inactivation under light has been reported by Foster et al., [4] and Tung and Daoud, [10]. More recently, our EPFL laboratory has reported in a detailed way the partial damage/degradation of the *E. coli* outer cell functional groups during TiO₂ photocatalysis by ATR-IR spectroscopy [50, 66].

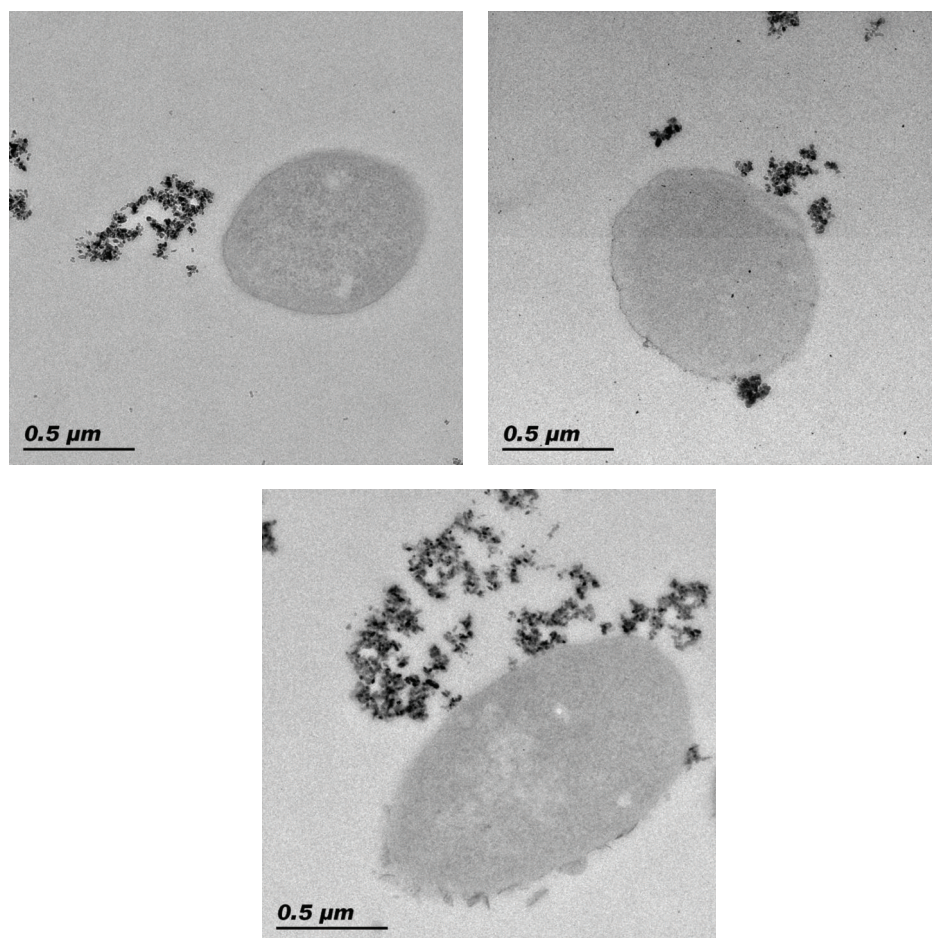


FIGURE 15: TEM biomicroscopy of TiO₂-polyester 5% (HT) interacting with the *E. coli* cell wall in the dark: (i) upper left hand side: time zero, (ii) upper right hand side: time 30 min, and (iii) central lower position: time 120 min. For more details see text.

By X-ray diffraction spectroscopy (XRD) the TiO₂ crystalline phases on the 5% TiO₂-polyester prepared by the HT-method show a significant anatase (A) peak at $2\theta = 21.5^\circ$ and a small rutile peak at $2\theta = 37.3^\circ$. These XRD results showing the formation of anatase and rutile peaks are due to the structure forming function of the polyester at low temperatures when colloidal TiO₂ suspensions were added. When heating TiO₂ suspensions by themselves anatase was formed $\sim 300^\circ\text{C}$ and rutile at around 600°C in the absence of a structure forming surface like polyester [9, 12, 13]. These last temperatures are significantly higher compared to temperatures $\sim 80^\circ\text{C}$ required to prepare the TiO₂ with anatase and rutile phases as detected by XRD.

3.3.2. Transmission Electron Microscopy of the *E. coli* Cell Wall Interaction with TiO₂-Polyester. Sample Preparation and Process Kinetics. The samples of the TiO₂ polyester for the electron microscopy of the *E. coli* interaction with TiO₂-polyester fabrics were prepared in the following way: suspensions or *E. coli* were fixed in paraformaldehyde 2% + glut 0.2% in phosphate buffer for 30 min and centrifuged and pellet resuspended in low melting point agarose. This was then cut

into small cubes, dehydrated, and stained for 20 min in 2% uranyl acetate then dehydrated in a graded alcohol series. The samples were then embedded in LR white resin in Beam capsules and polymerized overnight at 55°C . The resin blocks containing the *E. coli* on TiO₂-polyester were thin sectioned to a 70 nm thickness with an ultramicrotome (Leica UC7). The TiO₂-polyester fibers were embedded in epoxy and thin sectioned at a thickness of 80 to 100 nm.

The transmission electron microscopy (TEM) of the TiO₂-polyester (HT) samples interacting with *E. coli* is shown in Figure 15. The TEM in the upper left corner in Figure 15 shows the interaction of TiO₂-polyester (HT) sample with the *E. coli* K12 at time zero. The *E. coli* intact cell wall is seen as well as the aggregates and coaggregates of TiO₂ positioned at a distance from the cell wall in agreement with the DLVO theory of colloidal stability. TiO₂ nanoparticle aggregation sets in at a pH close to the isoelectric point (IEP) of 6-7 due to the attractive Van der Waals forces leading to TiO₂ aggregation within 30 min as shown in the TEM in the upper right corner [76]. The TiO₂ single particles present sizes between 40 and 60 nm and the hydrodynamic diameter of the aggregates was found to be 170–240 nm equivalent to 3-4 primary TiO₂ particles. After 30 min, the TiO₂ aggregates

accumulate on the cell wall surface due to their almost neutral charge at physiological pH and this is shown in the right upper hand side Figure 15. Damage in the cell wall is localized in the contact area between the TiO₂ and bacteria due to (a) the weak attraction between the TiO₂ (IEP ~6-7) and the negatively charged cell wall. Damage in the cell wall was observed at a pH close to the TiO₂ IEP (charge zero). The TiO₂ particles aggregate between themselves since they have an almost neutral charge. Concomitantly the Van der Waals attractive forces drive the interaction between the TiO₂-aggregates and the bacterial cell wall and (b) damage to the cell wall is also possible due to the abrasion by the TiO₂ rutile component of the *E. coli* envelope [77]. The effect of the cell wall in the dark after 30 minutes seems to be critical step in the loss of bacterial viability.

The lower central TEM in Figure 15 shows the damage to the *E. coli* outer wall cell within 120 min. After 120 min the wall outer layers present discontinuities in some regions and vanished in other regions. Cell wall damages leading to cell inactivation involve changes in cell morphology, cell-wall microstructure, and local pH [78]. The extensive damage to the outer cell layers after 120 min coincides with the time required for the total loss of cell viability in the dark shown in Figure 13. The bacterial cell cannot function anymore as a membrane regulating the in and out osmotic pressure and material flow. Sunada et al. reported *E. coli* inactivation by TiO₂ films damaging the cell wall membrane due to the leakage of internal cell components [79].

4. Conclusions

- (i) This study accounts on self-disinfecting and self-cleaning TiO₂ films recently investigated in our laboratory. The design, preparation, evaluation, and characterization of uniform, adhesive, and innovative photocatalytic TiO₂ coatings are described.
- (ii) It is possible by traditional DC, DCP, and HIPIMS sputtering to produce antibacterial films on 2D and 3D objects at low temperature on polymer films and textile fabrics not resisting higher temperatures.
- (iii) The microstructure of TiO₂ films still has to be characterized to find the most suitable microstructure leading to disinfection in the minutes/seconds and not in hours.
- (iv) An interdisciplinary approach is necessary when working in the field of self-disinfecting coatings as presented in this study.
- (v) A considerable saving in Ti and deposition time (energy) was found with HIPIMS compared to conventional DC/DCP sputtering when coating surfaces.
- (vi) TiO₂-polyester surfaces have been shown in this study to inactivate bacteria in the dark. This is an important point not addressed generally in bacterial inactivation studies addressing mainly TiO₂ photocatalysis.

Conflict of Interests

The authors declare that there is no conflict of interests regarding the publication of this paper.

Acknowledgments

The authors thank the EPFL and Swiss National Science Foundation (SNF) Project (200021-143283/1) for financial support of this work and EPFL-CIME for their help with the electron microscopy experiments and the COST Actions MP1101 and I106 for interactive discussions during the course of this study.


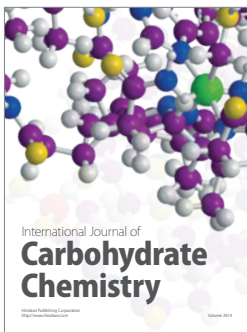
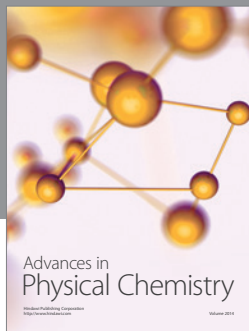
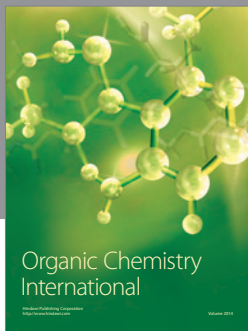
References

- [1] A. Kramer, I. Schwebke, and G. Kampf, "How long do nosocomial pathogens persist on inanimate surfaces? A systematic review," *BMC Infectious Diseases*, vol. 6, pp. 130–138, 2006.
- [2] K. Taylor, R. Roberts, and J. Roberts, *The Challenge of Hospital Acquired Infections (HAI)*, National Audit Office, 2002.
- [3] K. Page, M. Wilson, and I. P. Parkin, "Antimicrobial surfaces and their potential in reducing the role of the inanimate environment in the incidence of hospital-acquired infections," *Journal of Materials Chemistry*, vol. 19, no. 23, pp. 3818–3831, 2009.
- [4] H. A. Foster, I. B. Ditta, S. Varghese, and A. Steele, "Photocatalytic disinfection using titanium dioxide: spectrum and mechanism of antimicrobial activity," *Applied Microbiology and Biotechnology*, vol. 90, no. 6, pp. 1847–1868, 2011.
- [5] S. Pigeot-Rémy, F. Simonet, E. Errazuriz-Cerda, J. C. Lazzaroni, D. Atlan, and C. Guillard, "Photocatalysis and disinfection of water: identification of potential bacterial targets," *Applied Catalysis B: Environmental*, vol. 104, no. 3–4, pp. 390–398, 2011.
- [6] A. Fujishima, K. Hashimoto, and T. Watanabe, *TiO₂ Photocatalysis*, Bkc Inc. Pub. Co., Tokyo, Japan, 2000.
- [7] A. Mills and S. Lee, "A web-based overview of semiconductor photochemistry-based current commercial applications," *Journal of Photochemistry and Photobiology A: Chemistry*, vol. 152, pp. 233–247, 2002.
- [8] A. Fujishima, X. Zhang, and D. A. Tryk, "TiO₂ photocatalysis and related surface phenomena," *Surface Science Reports*, vol. 63, no. 12, pp. 515–582, 2008.
- [9] J. Kiwi and C. Pulgarin, "Nano-structured self-cleaning and bactericide textiles," in *Self-Cleaning Materials and Surfaces*, W. Daoud, Ed., chapter 7, pp. 205–224, Woodhead Publishing, Cambridge, UK, 2013.
- [10] W. S. Tung and W. A. Daoud, "Self-cleaning fibers via nanotechnology: a virtual reality," *Journal of Materials Chemistry*, vol. 21, no. 22, pp. 7858–7869, 2011.
- [11] J. Kiwi, S. Rtimi, and C. Pulgarin, "Cu, Cu/TiO₂ thin films sputtered by up to date methods on non-thermal thin resistant substrates leading to bacterial inactivation," in *Microbial Pathogens and Strategies For Combating Them: Science, Technology and Education*, A. Méndez-Vilas, Ed., vol. 1, pp. 74–82, Formatex Research Center, 2013.
- [12] A. Bozzi, T. Yuranova, and J. Kiwi, "Self-cleaning of wool-polyamide and polyester textiles by TiO₂-rutile modification under daylight irradiation at ambient temperature," *Journal of Photochemistry and Photobiology A: Chemistry*, vol. 172, no. 1, pp. 27–34, 2005.

- [13] A. Bozzi, T. Yuranova, I. Guasaquillo, D. Laub, and J. Kiwi, "Self-cleaning of modified cotton textiles by TiO₂ at low temperatures under daylight irradiation," *Journal of Photochemistry and Photobiology A: Chemistry*, vol. 174, no. 2, pp. 156–164, 2005.
- [14] J. Kiwi and C. Pulgarin, "Innovative self-cleaning and bactericide textiles," *Catalysis Today*, vol. 151, no. 1-2, pp. 2–7, 2010.
- [15] L. Zhang, R. Dillert, D. Bahnemann, and M. Vormoor, "Photo-induced hydrophilicity and self-cleaning: models and reality," *Energy & Environmental Science*, vol. 5, pp. 7491–7507, 2012.
- [16] H. A. Foster, D. W. Sheel, P. Sheel et al., "Antimicrobial activity of titania/silver and titania/copper films prepared by CVD," *Journal of Photochemistry and Photobiology A: Chemistry*, vol. 216, no. 2-4, pp. 283–289, 2010.
- [17] H. M. Yates, L. A. Brook, I. B. Ditta et al., "Photo-induced self-cleaning and biocidal behaviour of titania and copper oxide multilayers," *Journal of Photochemistry and Photobiology A: Chemistry*, vol. 197, no. 2-3, pp. 197–205, 2008.
- [18] P. S. M. Dunlop, C. P. Sheeran, J. A. Byrne, M. A. S. McMahon, M. A. Boyle, and K. G. McGuigan, "Inactivation of clinically relevant pathogens by photocatalytic coatings," *Journal of Photochemistry and Photobiology A: Chemistry*, vol. 216, no. 2-4, pp. 303–310, 2010.
- [19] L. A. Brook, P. Evans, H. A. Foster et al., "Highly bioactive silver and silver/titania composite films grown by chemical vapour deposition," *Journal of Photochemistry and Photobiology A: Chemistry*, vol. 187, no. 1, pp. 53–63, 2007.
- [20] S. J. Dancer, "The role of environmental cleaning in the control of hospital-acquired infection," *Journal of Hospital Infection*, vol. 73, no. 4, pp. 378–385, 2009.
- [21] L. Caballero, K. A. Whitehead, N. S. Allen, and J. Verran, "Inactivation of *Escherichia coli* on immobilized TiO₂ using fluorescent light," *Journal of Photochemistry and Photobiology A: Chemistry*, vol. 202, no. 2-3, pp. 92–98, 2009.
- [22] D. M. A. Alrousan, P. S. M. Dunlop, T. A. McMurray, and J. A. Byrne, "Photocatalytic inactivation of *E. coli* in surface water using immobilised nanoparticle TiO₂ films," *Water Research*, vol. 43, no. 1, pp. 47–54, 2009.
- [23] P. S. M. Dunlop, A. Galdi, T. A. McMurray, J. W. J. Hamilton, L. Rizzo, and J. A. Byrne, "Comparison of photocatalytic activities of commercial titanium dioxide powders immobilised on glass substrates," *Journal of Advanced Oxidation Technologies*, vol. 13, no. 1, pp. 99–106, 2010.
- [24] N. Farahani, P. J. Kelly, G. West, M. Ratova, C. Hill, and V. Vishnyakov, "Photocatalytic activity of reactively sputtered and directly sputtered titania coatings," *Thin Solid Films*, vol. 520, no. 5, pp. 1464–1469, 2011.
- [25] P. J. Kelly, P. M. Barker, S. Ostovarpour et al., "Deposition of photocatalytic titania coatings on polymeric substrates by HIPIMS," *Vacuum*, vol. 86, pp. 1880–1882, 2012.
- [26] Thüringer Surface and Biomaterials Kolloquium, Zeulenroda, Germany, September 2011.
- [27] The 22nd Annual BioInterface Conference, University College Dublin, Ireland, October 2012.
- [28] S. Rtimi, O. Baghriché, C. Pulgarin, J.-C. Lavanchy, and J. Kiwi, "Growth of TiO₂/Cu films by HIPIMS for accelerated bacterial loss of viability," *Surface and Coatings Technology*, vol. 232, pp. 804–813, 2013.
- [29] V. Kouznetsov, K. MacÁk, J. M. Schneider, U. Helmersson, and I. Petrov, "A novel pulsed magnetron sputter technique utilizing very high target power densities," *Surface and Coatings Technology*, vol. 122, no. 2-3, pp. 290–293, 1999.
- [30] J. Nogier, M. Delamar, P. Ruiz, K. Thampi, P. Albers, and J. Kiwi, "X-ray photoelectron spectroscopy of V₂O₅/TiO₂ catalysts," *Catalysis Today*, vol. 20, pp. 109–124, 1994.
- [31] D. Wagner, M. Riggs, E. Davis, and G. Müllenberg, Eds., *Handbook of X-Ray Photoelectron Spectroscopy*, Perkin-Elmer Corporation Physical Electronics Division, Eden Prairie, Minn, USA, 1979.
- [32] D. Shirley, "Corrections of electrostatic charged species in XPS-spectroscopy," *Physical Review B*, vol. B5, pp. 4709–4716, 1972.
- [33] P. M. Kumar, S. Badrinarayanan, and M. Sastry, "Nanocrystalline TiO₂ studied by optical, FTIR and X-ray photoelectron spectroscopy: correlation to presence of surface states," *Thin Solid Films*, vol. 358, no. 1, pp. 122–130, 2000.
- [34] C. Chan, T. Ko, and H. Hiroaka, "Polymer surface modification by plasmas and photons," *Surface Science Reports*, vol. 24, pp. 1–42, 1996.
- [35] M. I. Mejía, J. M. Marín, G. Restrepo et al., "Self-cleaning modified TiO₂-cotton pretreated by UVC-light (185 nm) and RF-plasma in vacuum and also under atmospheric pressure," *Applied Catalysis B: Environmental*, vol. 91, no. 1-2, pp. 481–488, 2009.
- [36] O. Baghriché, S. Rtimi, R. Sanjines, C. Pulgarin, and J. Kiwi, "Effect of the spectral properties of TiO₂, Cu, TiO₂/Cu sputtered films on the bacterial inactivation under low intensity actinic light," *Journal of Photochemistry and Photobiology A: Chemistry*, vol. 251, pp. 50–56, 2013.
- [37] K. Tennakone, C. T. K. Tilakaratne, and I. R. M. Kottegoda, "Photocatalytic degradation of organic contaminants in water with TiO₂ supported on polythene films," *Journal of Photochemistry and Photobiology, A: Chemistry*, vol. 87, no. 2, pp. 177–179, 1995.
- [38] J. Houska, S. Mraz, and J. M. Schneider, "Experimental and molecular dynamics study of the growth of crystalline TiO₂," *Journal of Applied Physics*, vol. 112, Article ID 073527, 2012.
- [39] J. Mathews, *Epitaxial Growth Part B*, IBM Thomas Watson Res. Center, Academic Press, New York, NY, USA, 1975.
- [40] Y. L. Jeyachandran and S. K. Narayandass, "The effect of thickness of titanium nitride coatings on bacterial adhesion," *Trends in Biomaterials and Artificial Organs*, vol. 24, no. 2, pp. 90–93, 2010.
- [41] R. Wang, K. Hashimoto, A. Fujishima et al., "Light-induced amphiphilic surfaces," *Nature*, vol. 388, no. 6641, pp. 431–432, 1997.
- [42] N. Sakai, R. Wang, A. Fujishima, T. Watanabe, and K. Hashimoto, "Effect of ultrasonic treatment on highly hydrophilic TiO₂ surfaces," *Langmuir*, vol. 14, no. 20, pp. 5918–5920, 1998.
- [43] T. Zubkoy, D. Stahl, T. L. Thompson, D. Panayotov, O. Diwald, and J. T. Yates Jr., "Ultraviolet light-induced hydrophilicity effect on TiO₂(110) (1×1). Dominant role of the photooxidation of adsorbed hydrocarbons causing wetting by water droplets," *Journal of Physical Chemistry B*, vol. 109, no. 32, pp. 15454–15462, 2005.
- [44] H. A. Foster, I. B. Ditta, S. Varghese, and A. Steele, "Photocatalytic disinfection using titanium dioxide: spectrum and mechanism of antimicrobial activity," *Applied Microbiology and Biotechnology*, vol. 90, no. 6, pp. 1847–1868, 2011.
- [45] R. K. Poole, C. Kumar, I. Salmon, and B. Chance, "The 650 nm chromophore in *Escherichia coli* is an "oxy"- or oxygenated compound, not the oxidized form of cytochrome oxidase d: an hypothesis," *Journal of General Microbiology*, vol. 129, no. 5, pp. 1335–1344, 1983.

- [46] M. C. van Loosdrecht, J. Lyklema, W. Norde, G. Schraa, and A. J. Zehnder, "The role of bacterial cell wall hydrophobicity in adhesion," *Applied and Environmental Microbiology*, vol. 53, no. 8, pp. 1893–1990, 1987.
- [47] C. Xu, D. Wellia, R. Amal, W. Liao, J. Loo, and T. Tan, "Fabrication of highly ordered TiO₂ nanorod/nanotube adjacent arrays for photoelectrochemical applications," *Langmuir*, vol. 2, pp. 1122–1128, 2010.
- [48] C. Gunawan, W. Y. Teoh, C. P. Marquis, J. Lifia, and R. Amal, "Reversible antimicrobial photoswitching in nanosilver," *Small*, vol. 5, no. 3, pp. 341–344, 2009.
- [49] D. Naumann, C. Schultz, A. Sabisch, M. Kastowsky, and H. Labischinski, "New insights into the phase behaviour of a complex anionic amphiphile: architecture and dynamics of bacterial deep rough lipopolysaccharide membranes as seen by FTIR, X-ray, and molecular modelling techniques," *Journal of Molecular Structure*, vol. 214, pp. 213–246, 1989.
- [50] J. Kiwi and V. Nadtochenko, "Evidence for the mechanism of photocatalytic degradation of the bacterial wall membrane at the TiO₂ interface by ATR-FTIR and laser kinetic spectroscopy," *Langmuir*, vol. 21, no. 10, pp. 4631–4641, 2005.
- [51] J. Pitha and N. Jones, "A comparison of optimization methods for fitting curves to infrared band envelopes," *Canadian Journal of Chemistry*, vol. 44, pp. 3031–3050, 1966.
- [52] J. Kiwi and V. Nadtochenko, "New evidence for TiO₂ photocatalysis during bilayer lipid peroxidation," *Journal of Physical Chemistry B*, vol. 108, no. 45, pp. 17675–17684, 2004.
- [53] I. W. Levin and E. N. Lewis, "Fourier transform raman spectroscopy of biological materials," *Analytical Chemistry*, vol. 62, no. 21, pp. 1101–1111, 1990.
- [54] S. Rtimi, C. Pulgarin, R. Sanjines, and J. Kiwi, "Innovative photo-switchable behavior by uniform, semi-transparent thin films leading to the reduction of environmental contamination under light," *RSC Advances*, vol. 3, pp. 16345–16349, 2013.
- [55] K. Sarakinos, J. Alami, and S. Konstantinidis, "High power pulsed magnetron sputtering: a review on scientific and engineering state of the art," *Surface and Coatings Technology*, vol. 204, no. 11, pp. 1661–1684, 2010.
- [56] S. M. Rosnagel and J. Hopwood, "Magnetron sputter deposition with high levels of metal ionization," *Applied Physics Letters*, vol. 63, no. 24, pp. 3285–3287, 1993.
- [57] F. Petronella, S. Rtimi, R. Comparelli et al., "Uniform In₂O₃/TiO₂ films effective in bacterial inactivation under low intensity solar irradiation," *Journal of Photochemistry and Photobiology A: Chemistry*, vol. 14, pp. 1–7, 2014.
- [58] S. Robin, T. Soulimane, and S. Lavelle, "Interactions of biofilm-forming bacteria with abiotic surfaces," *RSC Nanoscience and Nanotechnology*, vol. 21, pp. 122–135, 2012.
- [59] N. Novkovski and A. Tanuevski, "Origin of the optical absorption of In₂O₃ thin films in the visible range," *Semiconductor Science and Technology*, vol. 23, no. 9, Article ID 095012, 2008.
- [60] J. F. McCann and J. O'M Bockris, "Determination of electrochemical parameters of semiconductor materials," *Journal of The Electrochemical Society*, vol. 128, pp. 1719–1724, 1981.
- [61] W. Erbs, J. Kiwi, and M. Grätzel, "Light-induced oxygen generation in aqueous dispersion of In₂O₃ particles and determination of their conduction band position," *Chemical Physics Letters*, vol. 110, no. 6, pp. 648–650, 1984.
- [62] P.-V. Kamat, "Boosting the efficiency of quantum dot sensitized solar cells through modulation of interfacial charge transfer," *Accounts of Chemical Research*, vol. 45, pp. 1901–1915, 2012.
- [63] T. Matsunaga, R. Tomoda, T. Nakajima, and H. Wake, "Photoelectrochemical sterilization of microbial cells by semiconductor powders," *FEMS Microbiology Letters*, vol. 29, no. 1-2, pp. 211–214, 1985.
- [64] T. Saito, T. Iwase, J. Horie, and T. Morioka, "Mode of photocatalytic bactericidal action of powdered semiconductor TiO₂ on mutants streptococci," *Journal of Photochemistry and Photobiology B: Biology*, vol. 14, no. 4, pp. 369–379, 1992.
- [65] P.-C. Maness, S. Smolinski, D. M. Blake, Z. Huang, E. J. Wolfrum, and W. A. Jacoby, "Bactericidal activity of photocatalytic TiO₂ reaction: toward an understanding of its killing mechanism," *Applied and Environmental Microbiology*, vol. 65, no. 9, pp. 4094–4098, 1999.
- [66] R. Bacsa, J. Kiwi, T. Ohno, P. Albers, and V. Nadtochenko, "Preparation, testing and characterization of doped TiO₂ active in the peroxidation of biomolecules under visible light," *Journal of Physical Chemistry B*, vol. 109, no. 12, pp. 5994–6003, 2005.
- [67] P. K. J. Robertson, J. M. C. Robertson, and D. W. Bahnemann, "Removal of microorganisms and their chemical metabolites from water using semiconductor photocatalysis," *Journal of Hazardous Materials*, vol. 211-212, pp. 161–171, 2012.
- [68] P. Amezaga-Madrid, R. Sylveyra-Morales, L. Cordoba-Fierro, G. Nevarez-Moorillon, E. Miki-Yoshida, and J. Solis, "TEM evidence of ultrastructural alteration of *Pseudomonas aeruginosa* by photocatalytic TiO₂ thin films," *Journal of Photochemistry and Photobiology B*, vol. 44, pp. 45–50, 2003.
- [69] D. Mitoraj, A. Jańczyk, M. Strus et al., "Visible light inactivation of bacteria and fungi by modified titanium dioxide," *Photochemical and Photobiological Sciences*, vol. 6, no. 6, pp. 642–648, 2007.
- [70] C. Pagnout, S. Jomini, M. Dadhwal, C. Caillet, F. Thomas, and P. Bauda, "Role of electrostatic interactions in the toxicity of titanium dioxide nanoparticles toward *Escherichia coli*," *Colloids and Surfaces B: Biointerfaces*, vol. 92, pp. 315–321, 2012.
- [71] P. K. Stoimenov, R. L. Klinger, G. L. Marchin, and K. J. Klabunde, "Metal oxide nanoparticles as bactericidal agents," *Langmuir*, vol. 18, no. 17, pp. 6679–6686, 2002.
- [72] J. Diaz-Visurraga, G. Cardenas, and A. Garcia, "Morphological changes induced in bacteria as evaluated by electron microscopy," in *Microscopy Science, Technology, Applications*, A. Méndez-Vilas and J. Diaz, Eds., Formatex, Madrid, Spain, 2010.
- [73] C. Johansen, T. Gill, and L. Gram, "Antibacterial effect of protamine assayed by impedimetry," *Journal of Applied Bacteriology*, vol. 78, no. 3, pp. 297–303, 1995.
- [74] P. S. M. Dunlop, M. Ciavola, L. Rizzo, and J. A. Byrne, "Inactivation and injury assessment of *Escherichia coli* during solar and photocatalytic disinfection in LDPE bags," *Chemosphere*, vol. 85, no. 7, pp. 1160–1166, 2011.
- [75] J. Nestic, S. Rtimi, C. Pulgarin, G. M. Roglic, and J. Kiwi, "New evidence for TiO₂ nanoparticulate films inducing cell wall damage during the loss of bacterial viability in the dark," *Angewandte Chemie International Edition*. Submitted.
- [76] L. Zhukova, J. Kiwi, and V. Nikandrov, "Effect of TiO₂ nanoparticles on *E. coli* cell division capacity at pH 4.0–4.5 in the absence of UV-irradiation," *Journal of Colloid and Interface Science B: Biomaterials*, vol. 97, pp. 240–247, 2012.
- [77] L. Caballero, K. A. Whitehead, N. S. Allen, and J. Verran, "Inactivation of *Escherichia coli* on immobilized TiO₂ using fluorescent light," *Journal of Photochemistry and Photobiology A: Chemistry*, vol. 202, no. 2-3, pp. 92–98, 2009.
- [78] P. Vadgama, *Personal Communication, Clinical Biochemistry Biomedical Materials*, Queen Mary College, London University.

- [79] K. Sunada, T. Watanabe, and K. Hashimoto, "Studies on photokilling of bacteria on TiO₂ thin film," *Journal of Photochemistry and Photobiology A: Chemistry*, vol. 156, no. 1-3, pp. 227-233, 2003.



Hindawi

Submit your manuscripts at
<http://www.hindawi.com>

